CONF-860366--12

UCRL--94258

DE87 001432

UCRL-94258
PREPRINT

OPTICAL MODELING OF INDUCTION-LINAC DRIVEN FREE-ELECTRON LASERS

E. T. Scharlemann and W. M. Fawley

This paper was prepared for submittal to
SPIE 1986 Technical Symposium Southeast on
Optics and Optoelectronic Systems
31 March - 4 April 1986
Orlando, Florida

March 31, 1986

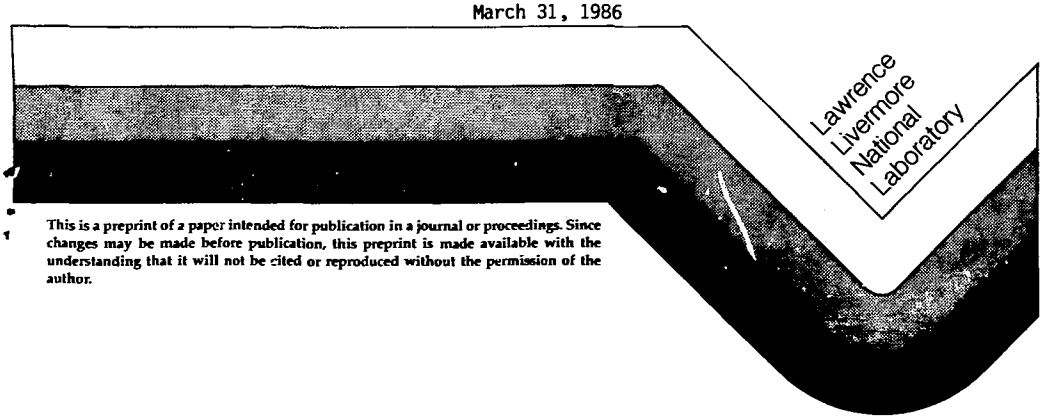

OPTICAL MODELING OF INDUCTION-LINAC DRIVEN FREE-ELECTRON LASERS*

E. T. Scharlemann and W. M. Fawley

Lawrence Livermore National Laboratory
University of California
Livermore, California

March 31, 1986

ABSTRACT

The free-electron laser (FEL) simulation code FRED, developed at Lawrence Livermore National Laboratory (LLNL) primarily to model single-pass FEL amplifiers driven by induction linear accelerators, is described. The main emphasis is on the modeling of optical propagation in the laser and on the differences between the requirements for modeling rf-linac-driven vs. induction-linac-driven FELs. Examples of optical guiding and mode cleanup are presented for a 50 μm FEL.

*Work performed jointly under the auspices of the U. S. Department of Energy by Lawrence Livermore National Laboratory under contract W-7405-ENG-48, for the U. S. Army Strategic Defense Command and the Department of Defense under Defense Advanced Resesarch Projects Agency Order No. 5316 in support of SDIO/USA-SDC MIPR No. W31-RPD-53-A127.

I. INTRODUCTION

In this paper we present a brief description of the free-electron laser simulation code FRED, developed at LLNL primarily for modeling single pass FEL amplifiers driven by induction linear accelerators.

Induction linacs differ from rf linacs in the kinds of FELs they can drive in the following ways: 1) the electron beam from an induction linac has relatively high peak current (multi-kA), therefore an induction-linac-driven FEL can have much higher gain per pass than an RF-linac-driven FEL; 2) the pulse repetition rate of an induction linac is much lower (< 1 kHz), and the pulse length is much greater (≈50 ns), so that oscillator configurations, in which the laser light remains in a resonator between electron beam pulses, are impractical. Instead, a single-pass amplifier configuration, driven by a master oscillator, is necessary. The high currents from an induction linac make this approach possible; 3) high gain and high current in an induction-linac-driven FEL permit the electron beam to guide the light over many Rayleigh ranges as if the electron beam were an optical fiber. As a consequence, the wiggler can (and often must, for high extraction efficiency) be much longer than a Rayleigh range. The current provided by present day RF linacs is too low to permit significant optical guiding, therefore the wiggler in an RF-linac-driven FEL must in general be less than two Rayleigh ranges long; 4) the higher current in an induction-linac-driven FEL does not come for free--the electron beam has much larger emittance (a measure of transverse beam temperature).

The physical differences between FELs driven by induction or RF linacs necessitate differences in the optical modeling. An induction-linac-driven FEL can have many dB of gain within a single optical Rayleigh range; together

with the very long wigglers (length L_w >> Rayleigh range z_R), the high gain argues strongly against either, 1) assuming an a priori optical field profile, or 2) working with an optical mode expansion--for example, numerically following the amplitudes of the lowest order modes of a resonant cavity. Instead, we feel that it is best to determine numerically an optical field profile $\varepsilon(r,z)$ on a radial grid, at each z step of a simulation, without the implicit assumptions about field profile contained in a mode expansion. The point, of course, is that the natural modes of an FEL amplifier can be very different from the normal modes of free space. At least 2D (r and z) modeling is required to treat diffractive and refractive effects; 3D modeling (r, ϕ, and z, or r, z, and t) is of course preferable, but much more expensive, computationally.

The development of FRED was begun[1,2] primarily to model diffractive and refractive effects produced by the electron beam. The particle motion in the present version of FRED has been described elsewhere;[3] we will concentrate here on a description of the field solver, which takes the current source term in the wave equation and solves for the slowly varying complex amplitude of the laser electric field. The equations solved by FRED are described in the next section (II); they are fairly standard in FEL modeling. (For an introduction to FEL physics, and a very good set of references, the reader is referred to Ref. 4.) The numerical technique used in the field solver is described in Section III. Examples of optical propagation in a 50 μm FEL, driven with a 1 kA electron beam from a 20 MeV induction linac, are presented in Section IV. The examples illustrate three optical phenomena expected from a high-gain single-pass amplifier: excellent output mode quality, rapid cleanup of a severely aberrated input from the master oscillator, and optical

guiding. Finally, recent modifications to the code which permit it to model three-dimensional optical phenomena are described in Section V.

No experimental verification of the optical modeling in FRED exists yet. The only relevant, very high gain experiments[5] have been at microwave frequencies in a waveguide, where diffractive and refractive effects are masked by the waveguide boundary conditions. Reference 6 describes the comparison with those experiments, a comparison that tests only the FEL physics, not the optical modeling. FRED has been extensively benchmarked with analytical theory[7] and compared with the FEL code FELEX, written recently at Los Alamos National Laboratory by Brian McVey.[8]

II. FEL OPTICAL EQUATIONS

The equations that describe the optical field in an FEL come from the usual paraxial wave equation, with a source term obtained from the current produced as the electrons wiggle in the periodic magnetic field of the wiggler:[9,10]

$$\frac{\partial \varepsilon}{\partial z} - \frac{i}{2k} \nabla^2 \varepsilon = \frac{eZ_o i a_w f_B}{2mc^2} J(r,z) \left\langle \frac{e^{-i\theta_j}}{\gamma_j} \right\rangle \tag{1}$$

Here $\varepsilon(r,z)$ is the normalized complex amplitude of the electric field component amplified in the FEL:

$$E_x(r,z) = \frac{\sqrt{2}mc}{e}^2 \varepsilon(r,z)\, e^{i(kz-\omega t)} \tag{2}$$

k is the wavenumber of the laser light, a_w is the normalized, dimensionless, r.m.s. vector potential of the wiggler:

$$a_w = \frac{eB_w}{\sqrt{2}mc} \quad \text{[MKS units]} \quad , \tag{3}$$

J is the current density, the angle brackets denote an average over N electrons in one or a few optical wavelengths, and

$$\theta_j = (k + k_w)z_j - \omega t \quad [j = 1, N] \tag{4}$$

is the longitudinal position of an electron with respect to the ponderomotive potential formed by the wiggle motion and a plane electromagnetic wave propagating at c. In terms of θ_j, the phase of an electron in the actual ponderomotive well is

$$\psi_j = \theta_j + \Phi \quad . \tag{5}$$

with Φ the phase of the electric field. The factor f_B is a coefficient that accounts for a reduction in coupling between electrons and light because of the longitudinal component (on the scale of an optical wavelength) of an electron's wiggle motion.[10] Z_0 is the ubiquitous impedance of free space.

The longitudinal variables γ_j and θ_j vary according to the equations[9,10,11]

$$\frac{d\gamma_j}{dz} = -\frac{a_w e_s f_B}{\gamma_j} \sin\psi_j \quad , \tag{6}$$

$$\frac{d\theta_j}{dz} = k_w - \frac{k_s}{2\gamma_j^2}\left[1 + a_w^2 - 2a_w a_s f_B \cos\psi_j\right] \quad , \tag{7}$$

where

$$e_s = |\varepsilon| = k a_s \quad . \tag{8}$$

The wiggler and laser field quantities, a_w and ε, can be functions of all three cylindrical coordinates r,ϕ, and z. Therefore, in all of these equations, a_w and ε are evaluated at the instantaneous position of each electron.

The source term in Eq. (1) assumes that the ponderomotive potential wells ("buckets") are nearly identical for a long enough distance that the correct source term in the full wave equation can be Fourier transformed to pick out the component at ω and k. That Fourier transform converts the sum of δ-function particle positions into an average over $\exp(-i\theta_j)$.

Equation (1) neglects the slippage between the electrons and the light in the wiggler; i.e., it assumes that the electrons and photons are both traveling at c. For modeling most FEL phenomena, this is a good approximation (the relative slip is at most a few mm). The sideband instability,[12] however, is suppressed when this approximation is made. The sideband instability is a trapped particle instability that arises from the coupling provided among ponderomotive wells by the light slippage, and can lead to the breakup of the optical pulse into very rapid temporal fluctuations. A sideband version of the code (named GINGER, of course) is presently being tested and will be described in a later publication.

III. NUMERICAL TECHNIQUE

The basic version of FRED is 2D, in that it follows a complex field amplitude $\varepsilon(r,z)$ that has no ϕ dependence [for free-space propagation; for propagation in a rectangular waveguide,[6] $\varepsilon = \varepsilon(x,z)$]. The basic version of FRED is therefore restricted to modeling axisymmetric optical phenomena.

$\varepsilon(r,z)$ is determined by Eq. (1), which is solved numerically with a finite element method (originally constructed by S. Doss and R. Gelinas). In the implementation of the finite element method in FRED, $\varepsilon(r,z)$ is considered to be formed from the sum of triangular basis functions $\alpha_i(s)$ (where $s = r^2$), with α_i peaked at the radial coordinate s_i, and falling linearly to zero at

adjacent grid points:

$$\alpha_i(s) = \frac{s - s_{i-1}}{s_i - s_{i-1}} \quad s_{i-1} < s < s_i \quad , \tag{9}$$

$$\alpha_i(s) = \frac{s_{i+1} - s}{s_{i+1} - s_i} \quad , \quad s_i < s < s_{i+1} \quad . \tag{10}$$

The grid in r, or s, is generally not linear; the grid points are finely spaced near the electron beam where good radial resolution is required, but become exponentially increasing in separation as r increases away from the electron beam.

Equation (1) is integrated radially over each $\alpha_i(s)$, to reduce the partial differential Eq. (1) for $\varepsilon(r,z)$ to a system of 2K coupled ordinary differential equations for $\mathrm{Re}[\varepsilon(s_i)]$ and $\mathrm{Im}[\varepsilon(s_i)]$, $i = 1,K$, where K is the number of grid points (typically 63-127). These 2K ordinary differential equations are coupled by the $\nabla_\perp^2\varepsilon$ term in Eq. (1), and indirectly, by the source term on the right hand side. The system of 2K equations has the form

$$A \cdot \frac{dY}{dz} = B \cdot Y + S \quad , \tag{11}$$

where Y is the 2K vector of field quantities $Y = \{\mathrm{Re}[\varepsilon(s_1)], \mathrm{Im}[\varepsilon(s_1)], \mathrm{Re}[\varepsilon(s_2)], \mathrm{Im}[\varepsilon(s_2)],\ldots\}$, S is the 2K vector of source terms, and A and B are 2K x 2K tridiagonal matrices. In this form, the 2K equations are solved with the Gear scheme,[13] specifically programmed (primarily by A. Hindmarsh at LLNL) for a block tridiagonal matrix.

The Gear scheme is a predictor-corrector integration technique that maintains an estimate of the error at each step, and thus can choose its own step size to satisfy a specified error criterion. Because the corrector step is

iterated, the numerical algorithm is fully implicit. The numerical solution to Eq. (1) has never shown any evidence for numerical instability.

We have tested the vacuum propagation modeled by FRED in a variety of ways; one of the most exacting is the modeling of the diffraction pattern formed by a uniform plane wave emerging from a hard circular aperture. Figure 1 shows the results from FRED at a distance corresponding to a Fresnel number of 5, for 50 μm light through a 2 mm (radius) aperture. The inset is an experimental, and more careful theoretical, determination of the diffraction pattern, from Ref. 14.

The FEL physics in FRED has been compared with the LLNL microwave FEL experiment at the Electron Laser Facility (ELF), as mentioned in the Introduction. ELF operates at 34.6 GHz (λ = 8.7 mm) in an oversized (3 x 10 cm) waveguide. The same field solver is used, but the waveguide sufficiently alters the propagation physics that we cannot claim any experimental verification of the optical field solver.

IV. SAMPLE RESULTS

In Figs. 2 through 5, we present examples of results from the code for a 50 μm FEL driven by a 20 MeV accelerator that provides a 1 kA electron beam. The figures illustrate predicted output beam quality (Fig. 2a,b), mode cleanup (Figs. 3a,b and 4a,b), and optical guiding (Fig. 5ab). In all three cases, the electron beam has a 1.84 mm radius (hard edge, with parabolic density profile in r) in the wiggler, the input laser light is focused at the wiggler entrance with a 2.2 mm beam waist (w_0), and the input power is 1 MW (peak--since the code follows only one or a few ponderomotive wells, it knows nothing about pulse lengths, repetition rates, or average powers). The wiggler period

is 5 cm. The wiggler length varies among the cases. The wiggler is untapered, and saturation occurs at ~1.2 m; after saturation, the output beam quality deteriorates. For illustrations of output beam quality (Figs. 2-4), the wiggler was taken to be only long enough to reach saturation. For illustrations of optical guiding (Fig. 5), the wiggler was 25 Rayleigh ranges (about 8 m) long, to illustrate that guiding continues after saturation.

Radial profiles of intensity and phase of the output light from the 50 μm FEL are shown in Fig. 2a [intensity, I(r)] and 2b [phase, Φ(r)], together with least-squares fits to a pure Gaussian TEM_{00} mode. The beam quality can be characterized by a Strehl ratio (= ratio of peak far-field intensity on axis, with and without aberrations) of 0.98, or by a fractional power in the TEM_{00} mode of over 97%. The high quality beam output is not a function of input beam quality (at least in the simulations). Figures 3a,b illustrate intensity and phase cross sections of a severely aberrated input beam from the master oscillator. The phase aberrations in Fig. 3b correspond to $\pm \lambda/2$ on a scale of 0.35 w_0. The FEL output, with the input of Fig. 3, is shown in Fig. 4--again, intensity (Fig. 4a) and phase (Fig. 4b) cross sections. The peak intensity at output is reduced by the input aberrations, but the output mode quality is nearly as good as in the absence of input aberrations (Strehl ratio of 0.94, 97% TEM_{00}). One can consider the mode cleanup shown here as a failure of the FEL to couple to the higher order modes contained in the input field of Fig. 3.

Finally, Fig. 5 illustrates optical guiding by which is commonly meant the nearly self-similar propagation of laser light over many Rayleigh ranges. Optical guiding can be caused either by gain focusing, or by the phase shift of the light produced by the bunched electron beam. Fig. 5a is a 3D plot of

intensity vs. r and z in a wiggler nearly 8 m long, or 25 Rayleigh ranges (based on the input beam waist). Fig. 5b plots the beam waist w_0 of the least-squares Gaussian fit as a function of z. Over many Rayleigh ranges, w_0 changes by less than a factor of two, even in the absence of gain. This optical guiding phenomenon is analytically understood[15,16] and has often been observed in numerical simulations.[1,17] It has yet to be tested experimentally.

V. 3D EXTENSIONS

FRED has recently been extended to permit modeling of non-axisymmetric light propagation. The primary purpose of the extension was to model the effects of misalignment between the input electron or laser beams and the magnetic axis of the wiggler.

Electron beams from induction linacs usually have equal horizontal and vertical emittances, and often have equal horizontal and vertical focusing in the wiggler, so that the light propagation can be considered nearly axisymmetric. Furthermore, for propagation over many Rayleigh ranges (as in Fig. 5), it is essential that the outer simulation boundary (where $\varepsilon \to 0$, hence the boundary is perfectly reflecting) be far enough from the electron beam to avoid spurious interference effects between reflected and outward propagating light. The non-linear radial gridding is thus preferable to uniform Cartesian gridding, to provide adequate field resolution near the electron beam.

For these two reasons, and because the required modifications to FRED were simplest, non-axisymmetric propagation effects were added by writing

$$\varepsilon(r,\phi,z) = \sum_{m=-M}^{M} \varepsilon_m(r,z)\, e^{-im\phi} \quad . \tag{12}$$

and solving for the $\varepsilon_m(r,z)$ in a manner identical [except for coefficients in the $\nabla_\perp^2 \varepsilon$ term of Eq. (1)] to the treatment of $\varepsilon(r,z)$ described in Section III.

Figure 6 shows one example of non-axisymmetric effects that occur when the electron beam is initially offset by 0.4 mm ≈ 20% of the beam radius. The electron beam undergoes one betatron oscillation (i.e., oscillation of the beam centroid in the focusing fields of the wiggler) across the magnetic axis. Contours of light intensity in Fig. 6a qualitatively illustrate the tendency of the light to follow the electron beam. Quantitatively, the same effect is shown in Fig. 6b, where the offset of the peak of the laser intensity is plotted with the offset of the electron beam centroid, both as functions of z. The light peak follows the electron beam centroid quite closely.

REFERENCES

1. D. Prosnitz, R. A. Haas, S. Doss, and R. J. Gelinas, in Physics of Quantum Electronics, Vol. 9 (Addison-Wesley, Reading, Mass., 1982) 1047.

2. W. M. Fawley, D. Prosnitz, E. T. Scharlemann, Phys. Rev. A30 (1984) 2472.

3. E. T. Scharlemann, Journ. Applied Phys. 58 (1985) 2154.

4. W. B. Colson and A. M. Sessler, Ann. Rev. Nucl. Part. Sci. 35 (1985) 25.

5. T. J. Orzechowski, B. R. Anderson, W. M. Fawley, D. Prosnitz, E. T. Scharlemann, S. M. Yarema, A. M. Sessler, D. B. Hopkins, A. C. Paul, and J. S. Wurtele, in Free Electron Lasers, Proceedings of the 7th International Free Electron Laser Conference, ed. E. T. Scharlemann and D. Prosnitz, (North Holland, Amsterdam, 1986) 144.

6. E. T. Scharlemann, W. M. Fawley, B. R. Anderson, and T. J. Orzechowski, ibid., 150.

7. J. LaSala, D. A. G. Deacon, and E. T. Scharlemann, ibid., 389.

8. B. McVey, ibid.,449.

9. D. Prosnitz, A. Szoke, and V. K. Neil, Phys. Rev. A24 (1981) 1436.

10. W. B. Colson, IEEE Journ. Quantum Electronics QE-17 (1981) 1417.

11. N. M. Kroll, P. L. Morton, M. R. Rosenbluth, IEEE Journ. Quantum Electronics QE-17 (1981) 1436.

12. N. M. Kroll and M. R. Rosenbluth, in Physics of Quantum Electronics, Vol. 7 (Addison-Wesley, Reading, Mass., 1980) 147

13. C. W. Gear, Comm. Assoc. Comput. Mach. 14 (1971) 176.

14. A. J. Campillo, J. E. Pearson, S. L. Shapiro, and N. J. Terrell,Jr., Appl. Phys. Lett. 23 (1973) 85.

15. G. T. Moore, Optics Communications 52 (1984) 46.

16. E. T. Scharlemann, A. M. Sessler, and J. S. Wurtele, Phys. Rev. Lett. 54 (1985) 1925.

17. P. Sprangle and C.M. Tang, Applied Physics Letters 39 (1981) 677; C.M. Tang and P. Sprangle, in Physics of Quantum Electronics, Vol. 9 (Addison-Wesley, Reading, Mass., 1982) 627.

FIGURE CAPTIONS

Fig. 1: The calculated diffraction pattern from a uniformly illuminated, hard-edged circular aperture, at a Fresnel number of 5 ($z = a^2/5\lambda$, where $a = 2$ mm is the aperture radius, and $\lambda = 50$ μm is the wavelength of the light). The inset presents experimental measurements [14] of the diffraction pattern and a calculation made with 1800 grid points with a code constructed specifically to model large Fresnel number diffraction effects.

Fig. 2: Radial profiles of the output intensity (a) and phase (b) at saturation of a 50 μm FEL driven by a 1 kA, 20 MeV electron beam. A least-squares fit to a pure Gaussian TEM_{00} mode is overlaid.

Fig. 3: Radial profiles of the input intensity (a) and phase (b) for a severely aberrated ($\pm\lambda/2$ phase errors on a scale of $0.35w_0$) beam from the master oscillator.

Fig. 4: Radial profiles of the output intensity (a) and phase (b) of the FEL at saturation, with the aberrated input of Fig. 3. The intensity is less than in Fig. 1, but the mode quality is as good.

Fig. 5: Illustrations of optical guiding of the laser light by the electron beam in the 50 μm FEL: a) a 3D plot of intensity vs. r and z, to illustrate qualitatively that the light propagates over 10 Rayleigh ranges in a nearly self-similar fashion; b) a plot of laser beam waist, from least-squares Gaussian fits to the laser profile, as a function of z in the wiggler. The near constancy of w_0 quantitatively illustrates the self-similar propagation.

Fig. 6: An example of three-dimensional effects to be expected. For this case, with the parameters of the simulation in Fig. 5, the electron beam was initially offset by 0.4 mm = 0.2 x (electron beam radius). Fig. 6a illustrates contours of laser intensity showing a bending of the light by the electron beam. Fig. 6b shows the same effect quantitatively; the position of the peak of the laser intensity profile is plotted with the position of the electron beam centroid, both as a function of z.

ETS/jc:0802c

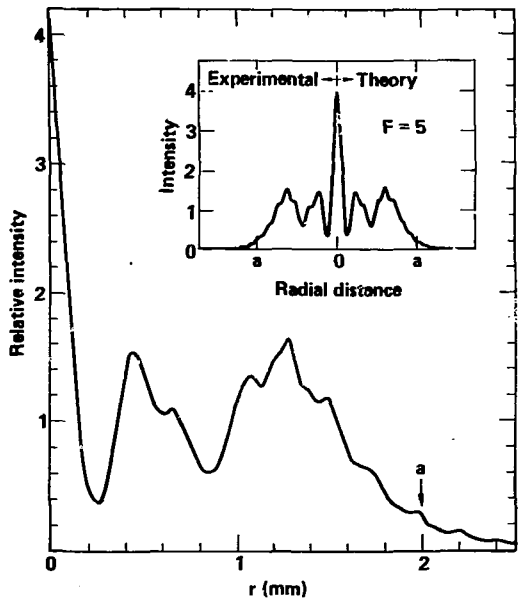
Experimental
Theory
F = 5
Intensity
Radial distance
a
0
a
Relative intensity
r (mm)
a

Figure 1.

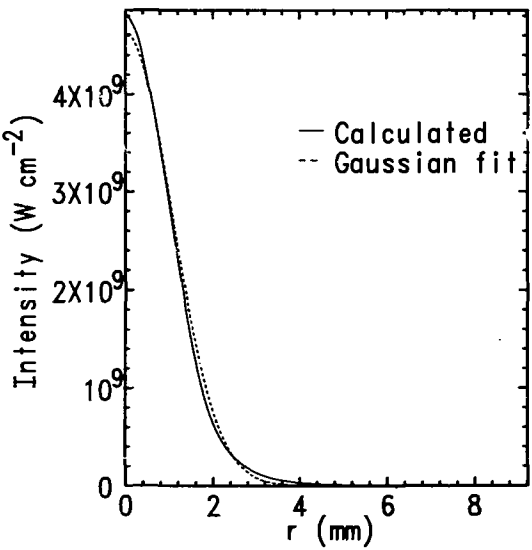
Intensity (W cm^{-2})
4X10^9
3X10^9
2X10^9
10^9
0
0
2
4
6
8
r (mm)
— Calculated
-- Gaussian fit

Figure 2a.

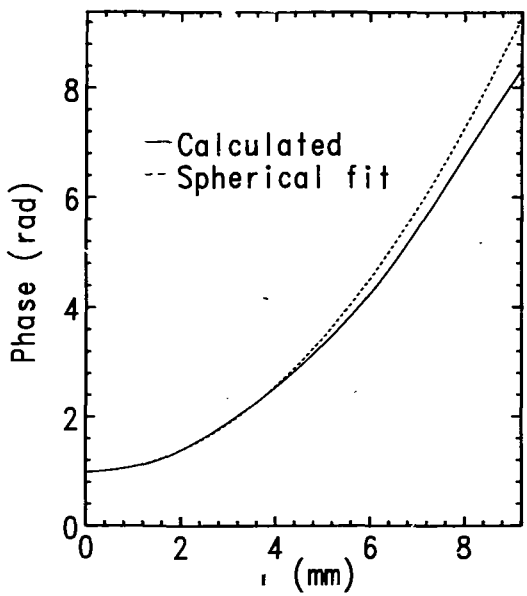

Figure 2b.

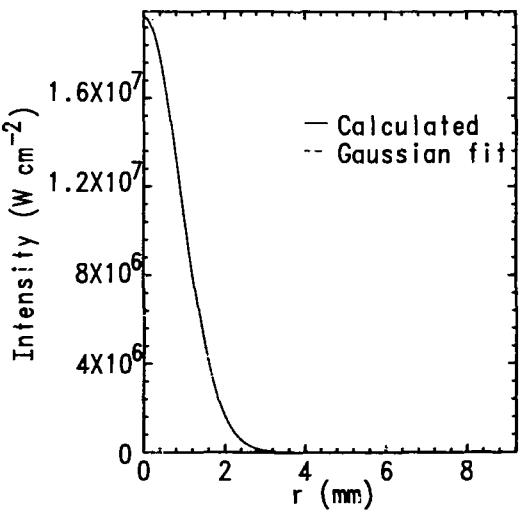
Intensity (W cm^{-2})
1.6X10^7
1.2X10^7
8X10^6
4X10^6
0
0
2
4
6
8
r (mm)
— Calculated
-- Gaussian fit

Figure 3a.

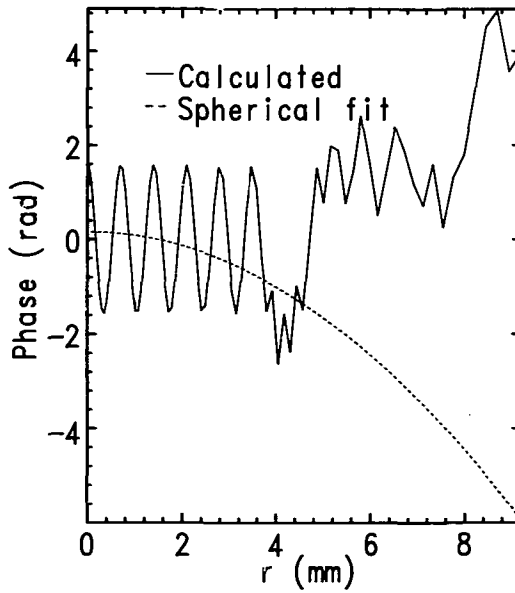

Figure 3b.

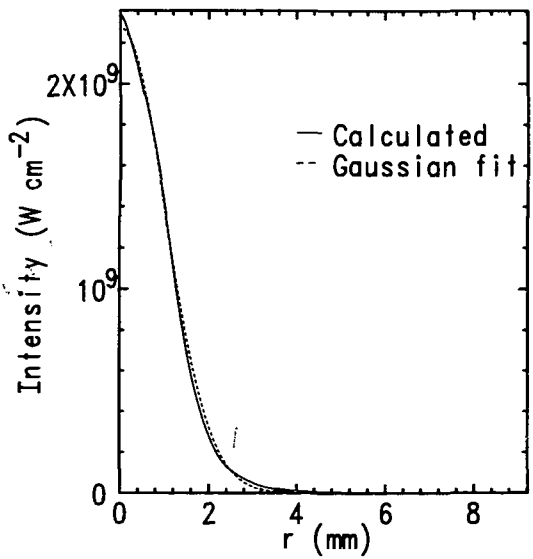
2X10^9
10^9
0
Intensity (W cm^-2)
— Calculated
-- Gaussian fit
0
2
4
6
8
r (mm)

Figure 4a.

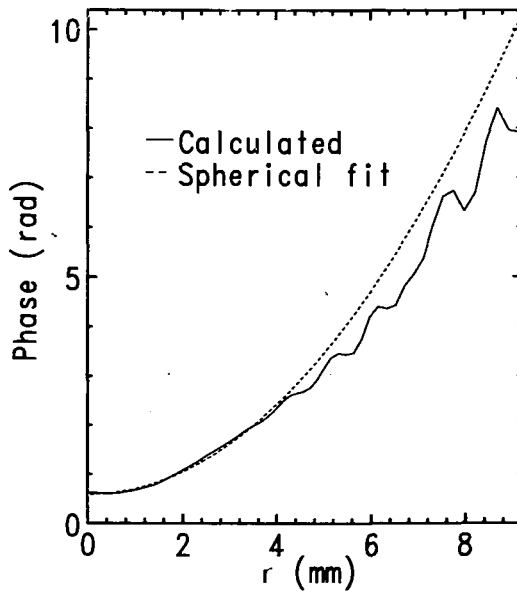

Figure 4b.

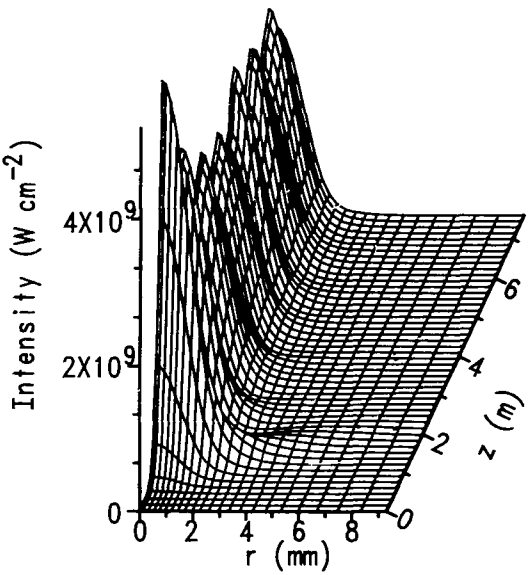

Figure 5a.

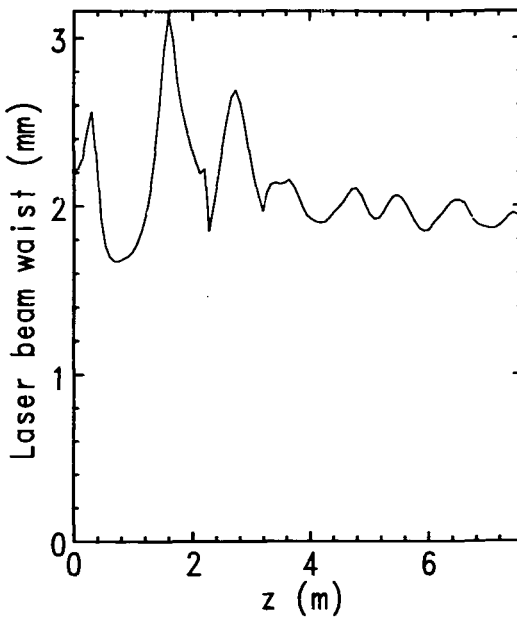

Figure 5b.

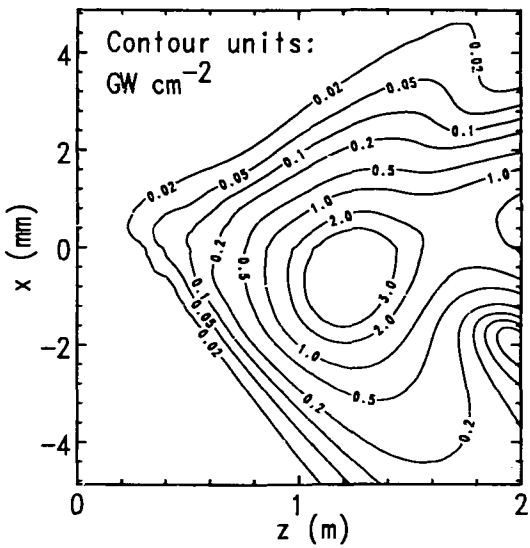

Figure 6a.

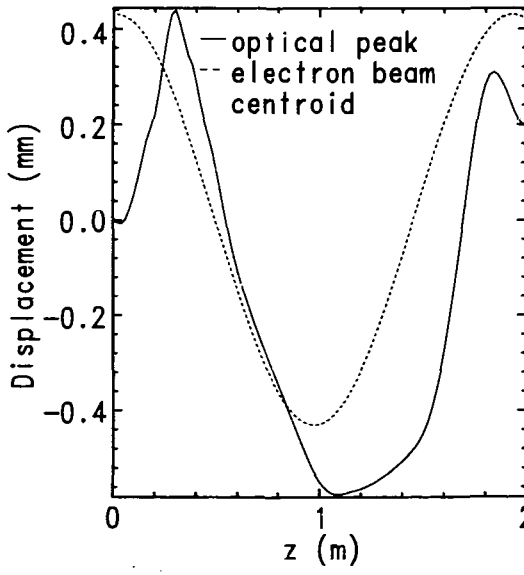
optical peak
electron beam centroid
Displacement (mm)
0.4
0.2
0.0
−0.2
−0.4
0
1
2
z (m)

Figure 6b.